Omni-directional reflectors for light-emitting diodes

Jong Kyu Kim*, J.-Q. Xi, and E. Fred Schubert
The Future Chips Constellation
Electrical, Computer and Systems Engineering Department
Rensselaer Polytechnic Institute, 110 Eighth Street, Troy, NY, USA 12180

ABSTRACT

This article discusses possible solutions to limitations in light extraction efficiency of light-emitting diodes (LEDs) using new types of triple-layer omni-directional reflectors (ODRs). The ODRs have lower mirror losses than metal reflectors and distributed Bragg reflectors (DBRs). High-reflectivity ODRs have been incorporated into AlGaInP LEDs and GaInN LEDs. It is shown that the ODR significantly increases light extraction from ODR-LEDs as compared to reference LEDs employing a DBR or metal reflector. Other examples of innovative concepts to be presented include novel materials with unprecedented low-refractive index, which further enhance the optical properties of ODRs.

Keywords: light-emitting diode, omni-directional reflector

1. Introduction

Waveguided optical modes occur in light-emitting diodes (LED) structures with a bottom and a top reflector. The bottom reflector can be a metal reflector, a distributed Bragg reflector (DBR) or an omnidirectional reflector (ODR). If the bottom reflector has the reflectivity R, the intensity of the light after N reflection events is given by R^N. Expressing this in terms of the mirror loss $L = 1 - R$, the intensity after N reflection events is given by $(1 - L)^N$ which, for low values of L, can be approximated by $(1 - L)^N \approx 1 - NL$. This equation shows that mirror losses should be kept at a minimum in high-efficiency LEDs.

There are several ways to obtain highly reflective coatings in the visible spectrum including metal mirrors, DBRs and ODRs, as shown in Fig. 1. Metal reflectors are robust reflectors capable of reflecting visible light over a wide range of wavelengths and incident angles. However, the reflectivity of Ag and Al is limited to ~ 95% in the visible wavelength region. DBRs are periodic structures with a unit cell of two dielectric layers having different refractive indices n_i and quarter-wavelength thicknesses d_i (i = 1, 2). However, the DBR reflectivity depends on the incidence angle θ such that the stop band shifts towards shorter wavelengths for increasing θ without changing its spectral width. As a result, DBRs become transparent for oblique-angles of incidence. Recently, triple-layer ODRs comprising a semiconductor with a refractive index n_s, a low-refractive index layer (n_{li}), and a metal with a complex refractive index $N_m = n_m + i\,k_m$, where k_m is the extinction coefficient, have been introduced. Triple-layer ODRs with high reflectivity, wide stop band, and omni-directional reflection characteristics have been demonstrated, and have shown the potential to outperform metal reflectors and DBRs. [1-3]

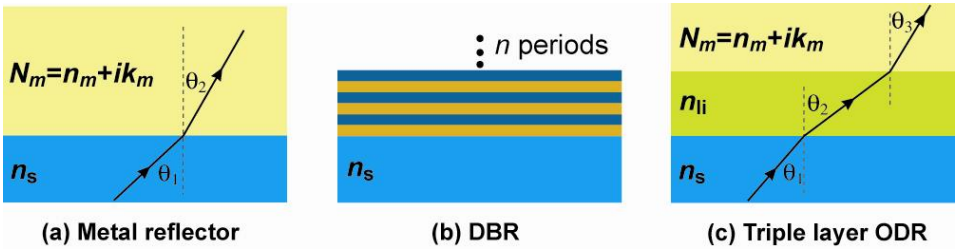

Fig. 1. Schematic cross-sectional view of (a) metal reflector, (b) distributed Bragg reflector (DBR), and (c) triple-layer omni-directional reflector (ODR).

* kimj4@rpi.edu; phone 1 518 276 6151; fax 1 518 276 8042

Light-Emitting Diodes: Research, Manufacturing, and Applications X,
edited by Klaus P. Streubel, H. Walter Yao, E. Fred Schubert, Proc. of SPIE Vol. 6134, 61340D, (2006)
0277-786X/06/$15 · doi: 10.1117/12.661563

In this paper, enhancements of light extraction in LEDs by using highly-reflective ODRs are presented. It is experimentally shown that the ODRs significantly increase the light extraction from the AlGaInP-based and GaInN-based LEDs as compared to reference LEDs employing a DBR or a metal reflector. Further improvements in reflectivity were achieved by using novel low-refractive index (low-n) materials such as nanoporous SiO_2 synthesized by a sol-gel process, and nanorod SiO_2 and indium-tin oxide (ITO) layer fabricated by oblique-angle deposition. It is shown that incorporation of low-n materials into LEDs results in enhanced reflectivity, and hence enhanced light-output of the ODR-LEDs due to a high refractive index contrast.

2. Theoretical calculation

The planar ODR consists of the LED semiconductor material emitting at a wavelength λ_0, a low refractive index layer (n_{li}) and a metal with a complex refractive index $N_m = n_m + ik_m$, where k_m is extinction coefficient. The reflectance of the semiconductor/metal reflector as a function of the incident angle θ is given by[4]

$$R_{TE} = \left| \frac{n_s \cos\theta_1 - N_m \cos\theta_2}{n_s \cos\theta_1 + N_m \cos\theta_2} \right|^2 \text{ and } R_{TM} = \left| \frac{\frac{n_s}{\cos\theta_1} - \frac{N_m}{\cos\theta_2}}{\frac{n_s}{\cos\theta_1} + \frac{N_m}{\cos\theta_2}} \right|^2 \quad (1)$$

The reflectance of the triple-layer ODR as a function of the incident angle θ is given by[4]

$$R = \left| \frac{r_{01} + r_{12} \exp(2i\phi)}{1 + r_{01} \cdot r_{12} \exp(2i\phi)} \right|^2 \quad (2)$$

where $r_{01TE} = \frac{n_s \cos\theta_1 - n_{li} \cos\theta_2}{n_s \cos\theta_1 + n_{li} \cos\theta_2}$, $r_{01TM} = \frac{n_{li} \cos\theta_1 - n_s \cos\theta_2}{n_{li} \cos\theta_1 + n_s \cos\theta_2}$, $r_{12TE} = \frac{n_{li} \cos\theta_2 - N_m \cos\theta_3}{n_{li} \cos\theta_2 + N_m \cos\theta_3}$, $r_{12TM} = \frac{N_m \cos\theta_2 - n_{li} \cos\theta_3}{N_m \cos\theta_2 + n_{li} \cos\theta_3}$, and $\phi = \frac{2\pi}{\lambda} n_{li} h \cos\theta_2$. Equation (2) applies to a low-index dielectric layer thickness of $\lambda_0/(4n_{li})$, i.e., to a quarter wavelength layer. Fig. 2 (a) compares the angular dependence of reflectivity of different triple-layer ODRs to a transparent DBR widely used in AlGaInP-based red LEDs emitting at 630 nm. In an AlGaInP-based LED (n_S = 3.3) emitting at 630 nm, Ag (n_{Ag}= 0.08, k_{Ag} = 4) is a particularly good choice as compared to Au (n_{Au}= 0.18, k_{Au} = 2.7). While the ODRs maintain high reflectivity at virtually all angles of incidence, the DBR reflectivity sharply drops above 17°. Fig. 2 (b) shows the angular dependence of the reflectivity of triple layer ODR ($GaN/SiO_2/Ag$), Ag, and 20 periods of $Al_{0.25}Ga_{0.75}N/GaN$ DBR at 470 nm (n_{Ag} = 0.132, k_{Ag} = 2.72, n_{SiO2} = 1.46, n_{GaN} = 2.45 at 470 nm). As opposed to the ODR and metal reflectors, R of the DBR sharply drops above 14° and recovers only at angles close to grazing incidence. Note that the reflectivity for TE-polarized light of the $GaN/SiO_2/Ag$ ODR is higher than that of the GaN/Ag reflector for all angles of incidence.

Because the LED active region emits light isotropically, the total substrate reflectivity averaged over the solid angle would be a suitable figure-of-merit. The average reflectivity is given by

$$R'(\lambda) = \frac{1}{2\pi} \int_0^{\pi/2} R(\lambda,\theta)\, 2\pi \sin\theta \, d\theta \quad (3)$$

where λ denotes the emission wavelength and θ the angle of incidence in the semiconductor. Values of R' for different reflectors are calculated by numerical integration of the reflectivity curves shown in Fig. 2 and are listed in Table I. The angle averaged reflectivity R' is much larger for a $GaN/SiO_2/Ag$ ODR (R' = 0.93 at λ = 470 nm) and Ag reflector (R' = 0.92 at λ = 470 nm) than for the DBR (R' = 0.49 for TE-polarized, R' = 0.38 for TM-polarized at λ = 470 nm). The averaged reflectivity of triple-layer ODRs exceeds the value of R' for the transparent DBR by about a factor of two. Note that the reflectivity increase is significant. The power of a wave-guided mode, P, attenuated by multiple reflection events (with reflectivity R) depends on the number of reflection events, N, according to $P = P_0 R^N$, where P_0 is the initial power of the mode.

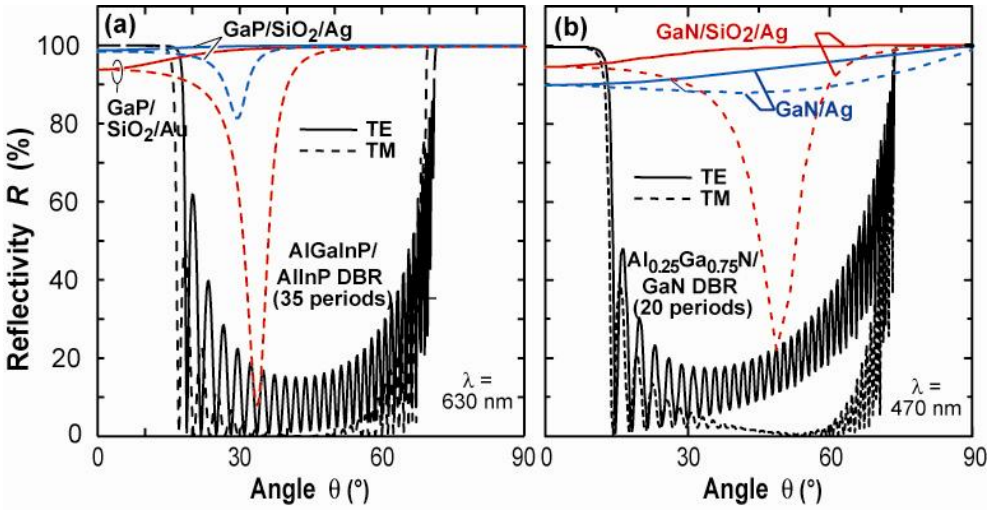

Fig. 2. (a) Calculated reflectivity R of triple layer ODR (GaP/SiO_2/Ag, GaP/SiO_2/Au and 35 periods of $(Al_{0.3}Ga_{0.7})_{0.5}In_{0.5}P$ /$Al_{0.5}In_{0.5}P$ DBR at λ = 630 nm. (b) Calculated reflectivity R of triple layer ODR (GaN/SiO_2/Ag), Ag reflector, and 20 periods of $Al_{0.25}Ga_{0.75}N$ /GaN DBR at 457 nm.

Table I. Values of the angle-integrated reflectivity R' at 630 nm for AlGaInP-based and at 470 nm for GaInN-based reflectors calculated from the reflectivity curves as shown in Fig. 2.

Reflector	n_m	k_m	R'
Ag/SiO_2/GaP	0.08	4	0.99 (630 nm)
Au/SiO_2/GaP	0.18	2.7	0.96 (630 nm)
AlGaInP DBR	2.9/3.35	-	0.47 (630 nm)
Ag/SiO_2/GaN	0.132	2.72	0.93 (470 nm)
Ag/GaN	0.132	2.72	0.92 (470 nm)
AlGaN DBR	2.5/2.2	-	0.49 (470 nm)

At perpendicular incidence, the reflectance of the triple-layer ODR is given by[2]

$$R_{\mathrm{ODR}}(\theta_1 = 0) = \frac{\{(n_{\mathrm{S}} - n_{\mathrm{li}})(n_{\mathrm{li}} + n_{\mathrm{m}}) + (n_{\mathrm{S}} + n_{\mathrm{li}})k_{\mathrm{m}}\}^2 + \{(n_{\mathrm{S}} - n_{\mathrm{li}})k_{\mathrm{m}} + (n_{\mathrm{S}} + n_{\mathrm{li}})(n_{\mathrm{li}} - n_{\mathrm{m}})\}^2}{\{(n_{\mathrm{S}} + n_{\mathrm{li}})(n_{\mathrm{li}} + n_{\mathrm{m}}) + (n_{\mathrm{S}} - n_{\mathrm{li}})k_{\mathrm{m}}\}^2 + \{(n_{\mathrm{S}} + n_{\mathrm{li}})k_{\mathrm{m}} + (n_{\mathrm{S}} - n_{\mathrm{li}})(n_{\mathrm{li}} - n_{\mathrm{m}})\}^2} \qquad (4)$$

For an AlGaInP/SiO_2/Ag structure emitting at λ = 630 nm, Equation (4) yields a normal-incidence reflectance $R_{\mathrm{ODR}}(\theta = 0) > 98$ %. This value exceeds the corresponding value for a structure *without* low-index layer by about 3 %, thereby reducing optical losses by a substantial amount. Due to the power-law dependence, this improvement of R is of great importance and shows the huge potential of ODRs.

3. Light-emitting diodes with omni-directional reflectors

3.1. AlGaInP LEDs with ODRs

An AlGaInP-based LED structure comprising a conductive ODR is presented and compared to a reference device employing a conductive DBR. Figure 3 shows top, cross-sectional and bottom view of the AlGaInP LED incorporating a conductive ODR. The AlGaInP LED consists of a top current-spreading layer, the active and confinement layers, a bottom window layer, the ODR, and a conductive holder such as a Si wafer. The active layers include the lower and upper confinement layers and the bulk or multiple-quantum well active region. The wafer is grown in the standard "p-side up" mode that is commonly employed for LEDs. The fabrication process includes deposition of the ODR, bonding of the wafer to a conductive holder such as Si, chemo-mechanical polishing for removal of the GaAs substrate, and metal contact deposition on the top window layer

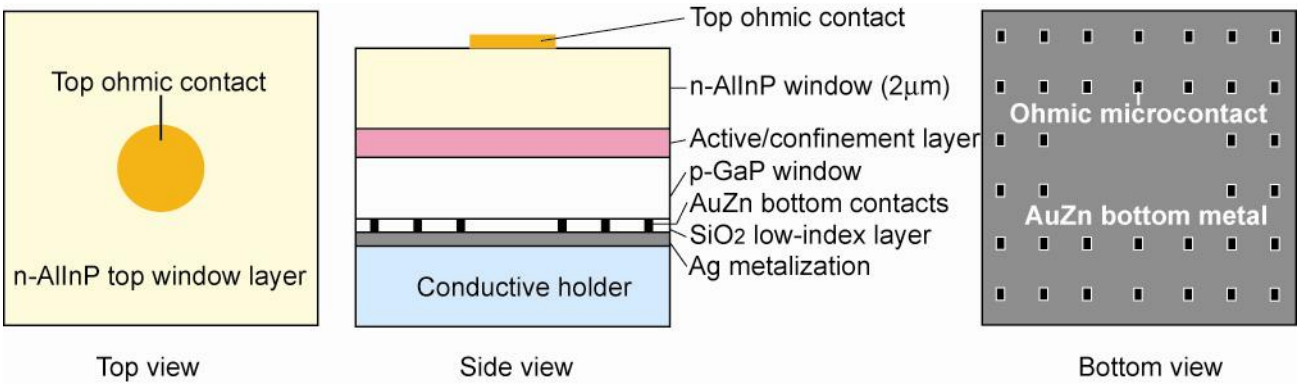

Fig. 3. A top view and a cross-sectional view, and a bottom view of the AlGaInP LED incorporating a conductive ODR. The original GaAs substrate has been removed and the LED is bonded "p-side down" to a new conductive holder. The ODR serves as p-type contact to the LED.

The current-voltage (*I-V*) characteristics of AlGaInP LEDs are shown in Fig. 4(a). Commercial AlGaInP absorbing-substrate (AS) LED emitting at 630 to 650 nm, and transparent-substrate (TS) LED emitting at 595 nm[5] are used as references. At a current of 20 mA, the forward voltage of the ODR-LED is about 2.7 V. Optical output power *P* versus injection current *I* for an ODR-LED, an AS LED with a DBR, and a TS-LED is shown in Fig. 4(b). The peak wavelengths of the three devices are 650 nm (ODR-LED), 630 nm (DBR-LED), and 595 nm (TS-LED) with junction areas $A_j \approx 0.09$, 0.25, and 0.05 mm^2, respectively. In order to measure the total optical output power the samples were placed on a reflecting holder inside an integrating sphere. The largest light output is attained by the ODR-LED. Maximum values of the external quantum efficiencies η_{ext} are about 18 % for the ODR-LED (I_f = 27 mA), 11 % for the DBR-LED (I_f = 11 mA). TS-LEDs operating at 632 nm have an external quantum efficiency of 32 %.[6] The external quantum efficiency of the ODR device is expected to further increase with a thicker top window layer. The window layer thickness of the ODR device shown in Fig. 3 is 2 μm and it is reasonable to expect an improvement by a factor of 2 for ODR devices with a thick window layer.

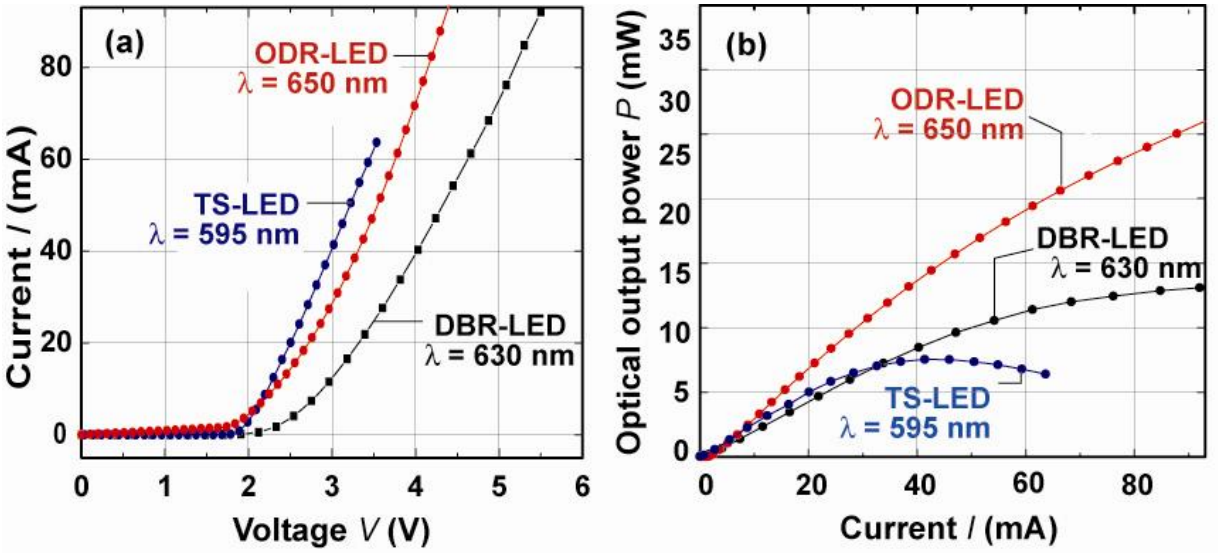

Fig. 4. (a) Current vs. voltage characteristics and (b) the dependence of the total optical output power on the drive current for ODR-, DBR-, and TS-AlGaInP LEDs emitting at 650, 630, and 595 nm, respectively. The junction areas A_j are about 0.09 mm^2 for ODR- and DBR-LEDs and about 0.05 mm^2 for the TS-LEDs.

3.2. GaInN LEDs with ODRs

A new ODR structure has been incorporated into GaInN blue LED as p-type ohmic contact.[3] The ODR comprises GaN, a thin layer of oxidized Ruthenium (Ru) used as semitransparent low-resistance p-type ohmic contact, a quarter-wave thick SiO_2 low-refractive index layer perforated by an array of Ag micro-contacts, and a thick Ag layer. The GaInN LED structure was grown by metal-organic chemical vapor deposition on c-plane sapphire substrate and consists of a thick n-type GaN buffer layer, an n-type GaN lower cladding layer, a GaInN/GaN multiple quantum well active region, a p-type GaN upper cladding, and a highly doped contact layer. LED mesa structures were obtained by standard photolithographic patterning followed by dry-etching to expose the n-type cladding layer. After 10 min dip in aqua regia solution to remove native oxide on p-type GaN, Ru (50 Å) was deposited and annealed at 500 °C under O_2 ambient to form RuO_2 acting as ohmic contact to p-type GaN. The RuO_2 obtained by this oxidation annealing was virtually colorless and transparent. Quarter wave thick SiO_2 was deposited on the RuO_2 using plasma-enhanced chemical vapor deposition. Then, an array of circular micro-contacts was patterned on SiO_2 and etched using HF solution to expose the conducting RuO_2 layer. Ag (200 nm) and Au (20 nm) were deposited on the top of the SiO_2 with perforated micro-contact holes by electron-beam evaporation at a pressure lower than 5×10^{-7} Torr. For comparison, LEDs with conventional Ni/Au and Ag contacts were fabricated on same wafer. The n-type contacts for the samples were fabricated by electron beam evaporation of Ti/Al/Ni/Au contacts without oxide removal or subsequent annealing.

Figure 5 shows a top view and a schematic cross-sectional view of the GaInN LED with GaN/RuO_2/SiO_2/Ag ODR. The dashed line in top view represents the cross-sectional cut shown in cross-sectional view. The chip dimensions are 300×300 μm^2. There is an array of circular micro-contacts in the p-contact area, enabling electrical conductivity between RuO_2 contact layer and Ag through insulating SiO_2 low-index layer. The radius of the micro-contacts is 4 μm. Because the RuO_2 contact layer, one of the conducting metal oxides, has advantages such as a low resistivity (~ 50 μΩcm) and a high work function (> 5 eV), it is expected to be an excellent current spreading and contact layer to p-type GaN with low contact resistivity.

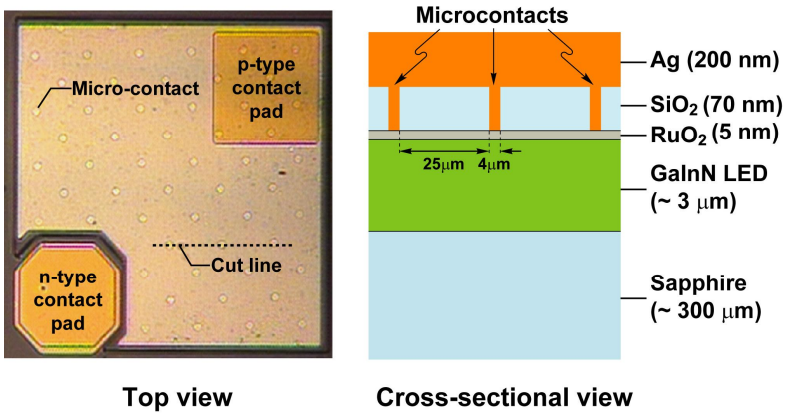

Fig. 5. A top view and a schematic cross-sectional view of the GaInN LED with GaN/RuO_2/SiO_2/Ag ODR. The SiO_2 low-refractive-index layer is perforated by micro-contacts enabling electrical conductivity between the RuO_2 contact layer and Ag.

Figure 6(a) shows *I-V* characteristics of the LED with GaN/RuO_2/SiO_2/Ag ODR and the conventional LEDs with Ni/Au and Ag contacts. The forward voltage at 20 mA for the LED with GaN/RuO_2/SiO_2/Ag ODR is 4.0 V, comparable to that of the conventional LED with Ni/Au contact, 3.9 V. This indicates that the contact resistivity of RuO_2 on p-type GaN is comparable to that of Ni/Au. On the other hand, the forward voltage of the LED with Ag contact is as high as 6.5 V. This is due to a low work function of Ag, resulting in a high potential barrier between Ag and p-type GaN. The electroluminescence intensity from the backsides of the LEDs was measured directly on a large-size (10×10 mm^2) Si PIN photodetector. The light-output–versus-current characteristic of the LEDs is shown in Fig. 6(b). At small forward currents ($I < 20$ mA), the light power extracted from the LED with ODR is slightly larger than the output from the LED with Ag contact, but significantly larger than that from the LED with Ni/Au contact. The increased light output of the LED with ODR can be attributed to higher reflectivity, and hence better light extraction efficiency due to the use of the ODR. In addition, a saturation of the light output power with increasing current level is not observed for the LED with GaN/RuO_2/SiO_2/Ag ODR, indicating that the resistivity of the RuO_2 layer and specific contact resistance of the GaN/RuO_2 contact is low enough for LED applications.

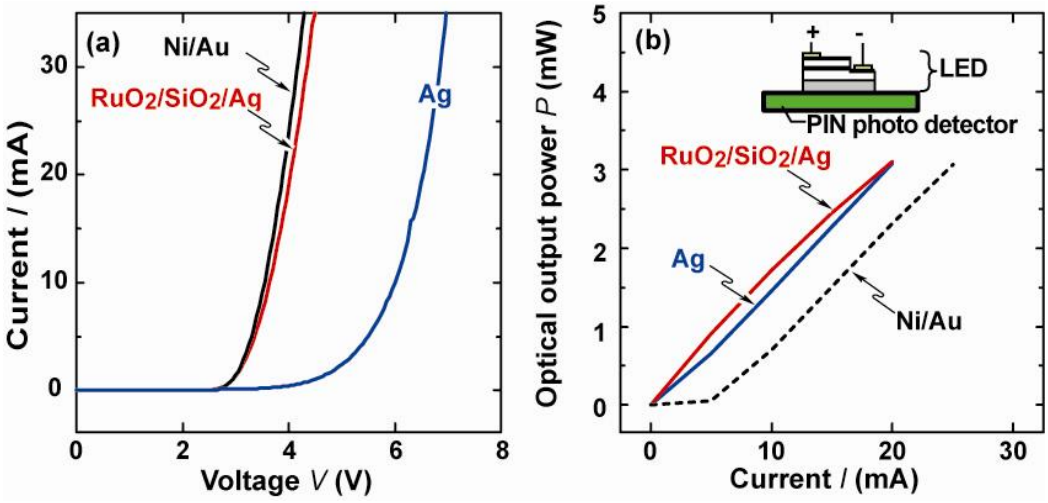

Fig. 6. (a) Current-voltage characteristics and (b) light output versus drive current characteristic of GaInN LEDs with GaN/RuO_2/SiO_2/Ag ODRs and LEDs with Ni/Au and Ag contacts.

3.3. ODRs with high refractive index contrast

The triple-layer ODR can be considered as a degenerate hybrid DBR/metal reflector. For DBRs, the reflectivity and spectral width of the high-reflectivity stop band directly depend on the refractive index contrast, i.e. the difference in refractive index between the high-index and low-index material. The higher the refractive index contrast, the higher the reflectivity, and the wider the spectral width of the stop band. Reducing the refractive index of the low-refractive-index layer, and hence increasing the refractive index contrast would further improve the reflectivity of ODRs. This motivates the development of new optical thin-film materials with low refractive index (low-*n*) and high transparency. Low-*n* materials can be obtained by several methods including (i) synthesis of nanoporous materials by sol-gel process and (ii) deposition of nanorod layer by oblique-angle deposition technique.

3.3.1. ODRs with nanoporous SiO_2 low-*n* layer by sol-gel process

The triple-layer ODR can be improved significantly by using novel low-*n* materials such as nanoporous SiO_2. The nanoporous SiO_2 was fabricated by sol-gel process with some modifications to suit the very small optical thickness and little scattering requirements.[7] GaP was treated in oxygen plasma to enhance the adhesion between the sol and substrate which originally has a hydrophobic surface property. The sol-gel solution was spun on the plasma treated GaP. To minimize Rayleigh scattering, Nitta *et al.*[7] and Xi *et al.*[8] have developed processes including a good control over evaporating rate by saturation of the atmosphere around the spin coater and aging of the spun-on film in the aging solution in an oven after spin coating. This yields an excellent average pore size of ~2 nm. Surface modification of nanoporous SiO_2 was then performed using hexamethyl disilazane (HMDS), which does not affect the adhesion of nanoporous SiO_2 film to the substrate. A 500 nm thick Ag layer was deposited by electron-beam evaporation.

The refractive indices at $\lambda = 632.8$ nm of the nanoporous SiO_2 and dense SiO_2 were determined by ellipsometer with Cauchy's formula as 1.23 and 1.46, respectively. The optimal thickness h_{opt} of the low-index layer for constructive interference at normal incidence is derived from

$$2\beta + \theta_{normal} = \frac{4\pi}{\lambda} n_{li} h_{opt} + \theta_{normal} = 2\pi \tag{5}$$

where, $\beta = (2\pi/\lambda) n_{li} h$. The phase change at the metal/dielectric interface for normal incidence satisfies

$$\tan\theta_{normal} = \frac{2\kappa_m n_{li}}{n_m^{\,2} + \kappa_m^{\,2} - n_{li}^{\,2}}. \tag{6}$$

The values of h_{opt} are determined to be 104 nm for the nanoporous SiO_2 layer and 84 nm for the dense SiO_2 layer. The actual thicknesses of the nanoporous SiO_2 and the dense SiO_2, measured by ellipsometer, are 105 nm and 89 nm, respectively.

The reflectivity *R* of the triple-layer ODR with SiO_2 as dielectric material layer is shown in Fig. 7(a). The near-normal incidence ($\theta = 1.2°$) TE and TM wave reflectivity is 97.3 % and 97.4 %, respectively. The calculated TE

reflectivity increases with angle with the lowest reflectivity, 98.1 %, at normal incidence, and reflectivities larger than 99.9 % for angles $\theta > 51°$. The calculated TM reflectivity has a Brewster-like dip with a minimum value of 74.2 % at $\theta = 30.4°$ and values exceeding 99.9 % for $\theta > 56°$. It can be calculated from Equation (3) that the ODR employing dense SiO_2 has an angle-integrated reflectivity $R'_{TE} = 99.8$ % and $R'_{TM} = 97.8$ %. For the ODR with nanoporous SiO_2, TE reflectivity of 97.6 % and TM reflectivity of 97.7 % are measured at near-normal incidence ($\theta = 1.2°$), as shown in Fig 7(b). Within the measured range, the TE reflectivity does not show a strong angular dependence. However, the TM reflectivity exhibits a Brewster-like dip near 27°. The experimental results closely follow the calculated reflectivity shown as solid lines in Fig. 7. The calculated TE polarization reflectivity increases with angle with the lowest reflectivity, 98.6 %, at normal incidence, and reflectivities larger than 99.9 % for angles $\theta > 47°$. The calculated TM polarization reflectivity has a Brewster-like dip with a minimum value of 80.0 % at $\theta = 25.1°$ and values exceeding 99.9 % for $\theta > 46°$. It can be calculated from Equation (3) that the triple-layer ODR employing nanoporous SiO_2 has an outstanding angle-integrated reflectivity $R'_{TE} = 99.9$ % and $R'_{TM} = 98.9$ %. This indicates that the mirror loss of nanoporous SiO_2 ODRs is a factor of 2 lower than that of dense SiO_2 ODRs.

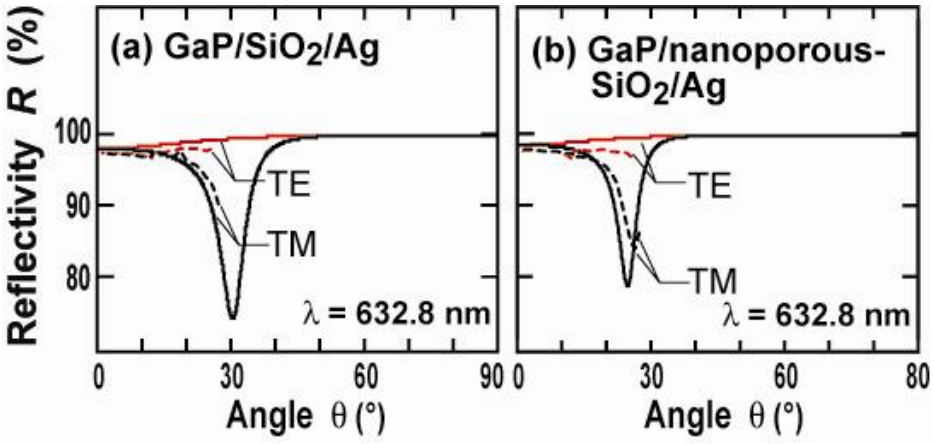

Fig. 7. Calculated (solid line) and measured (dotted line) reflectivity of (a) GaP/SiO_2/Ag and (b) GaP/nanoporous SiO_2/Ag triple-layer ODRs at $\lambda = 632.8$ nm.

3.3.2. ODRs with nanorod SiO_2 low-*n* layer by oblique-angle deposition

Although nanoporous SiO_2 with refractive index of 1.23 have been demonstrated for quarter-wave layers,[8] and even lower index of 1.14 were demonstrated for thicker layers,[9] spin-on sol-gel processes are not easily suitable for very thin and very low index layers. Here, optical films consisting of an array of SiO_2 nanorods with a refractive index as low as $n = 1.08$ are demonstrated and shown to have viable optical properties thereby making them very desirable for many applications.[10] Oblique-angle deposition is a technology to grow thin film with porous-microstructure caused by self-shadowing during the deposition process.[11, 12] Fig. 8(a) shows the deposition principle of oblique-angle deposition. A random growth fluctuation on the substrate produces a shadow region where the subsequent incident vapor flux cannot reach and a high edge where incident flux may deposit preferentially, creating an oriented rod-like structure. Therefore, in order to grow highly porous thin films, the incidence angle of the vapor flux, θ, has to be large.[8]

The optical micrograph of a low-*n* SiO_2 nanorod-array film deposited on a Si substrate is shown in Fig. 8(b) along with a scanning electron micrograph (SEM) showing the top view and the cross section of the film in Fig. 8(c). The optical micrograph reveals a smooth specular surface with no indication of scattering. The cross-sectional SEM clearly shows the angled array of SiO_2 nanorods. The gap between the SiO_2 nanorods is ≤ 50 nm, i.e. much smaller than the wavelength of visible light, and thus sufficiently small to make optical scattering very small. The SEM top view shows the nanostructure of the film including openings between the nanorods. For a deposition angle of 80 ° and a deposition rate of 2 Å/s, the growth direction of the nanorods is about 45 °, both angles being measured with respect to the surface normal of the sample. Since the film is deposited by evaporation, the controllability of film thickness is excellent, very suitable for deposition of very thin, around the quarter wavelength of visible light, optical films. Therefore, the oblique-angle deposition technology is very promising to grow optical coating films with very low refractive index for ODR fabrication.

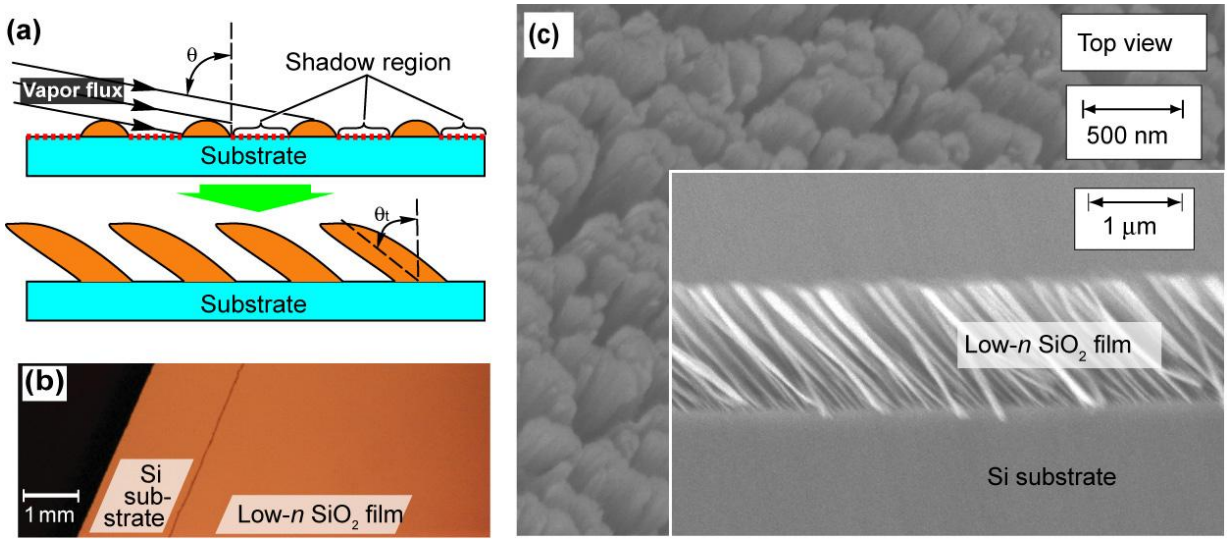

Fig. 8. (a) Schematic of oblique-angle deposition. (b) Optical micrograph of low-*n* SiO_2 nanorod-array film deposited on a Si substrate. (c) Scanning electron micrograph showing array of SiO_2 nanorods.

The experimental optical reflectivity of the low-*n* SiO_2 nanorod-array film is shown as a function of wavelength in Fig. 9(a). The reflectivity reveals periodic thin-film oscillations. Simulations of the reflectivity reveal that the thin-film interference oscillations are fully consistent with a refractive index of 1.08 and a thin-film thickness of 1.35 μm. These values were confirmed by both, ellipsometry measurements and thin-film thickness measurements using SEM. The ellipsometry model assumes a Cauchy-type layer on a Si substrate. The model fits the measurement data very well with mean square error of 4.92. The refractive index versus wavelength is shown in Fig. 9(b). Within the visible spectrum, the refractive index of the SiO_2 nano-rod layer is extremely low, namely $n = 1.09$.

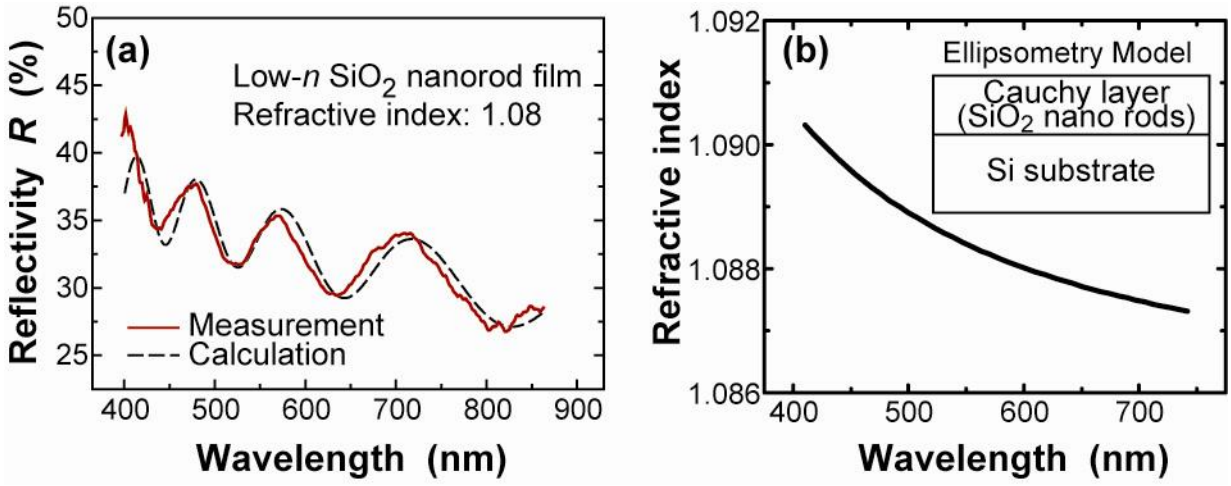

Fig. 9 (a) Thin-film reflectivity versus wavelength of SiO_2 nanorod-array film. Theoretical thin-film interference simulations reveal a refractive index of 1.08. (b) The refractive index of the SiO_2 nano-rod layer with wavelength measured by ellipsometry. The refractive index is $n < 1.09$ within the visible wavelength region.

To demonstrate the viability of the films for use in multilayer structures, we have fabricated a one-pair DBR consisting of a quarter-wave Si layer and a quarter-wave low-*n* SiO_2 layer deposited on a Si substrate. A critical step in the deposition is a surface-sealing step in which a very thin SiO_2 nano-rod array layer is grown on top of the low-*n* film. The nanorod orientation of the sealing film is near perpendicular to the orientation of the main film, thereby reducing the ability of a material deposited on top of the low-*n* film to enter the low-*n* film.

Figure 10(a) is the SEM of the Si/SiO_2 nano-rod DBR. The cross-sectional view clearly shows that the e-beam-deposited Si is located on the pore-closure layer on the SiO_2 nano-rod layer, forming a sharp interface between them. Although the top view of the DBR shows some texture, the feature size is too small to affect the optical properties of the Si layer. The root-mean-square (rms) surface roughness of the Si/SiO_2 nano-rod DBR is measured to 5.2 nm by atomic force microscopy.

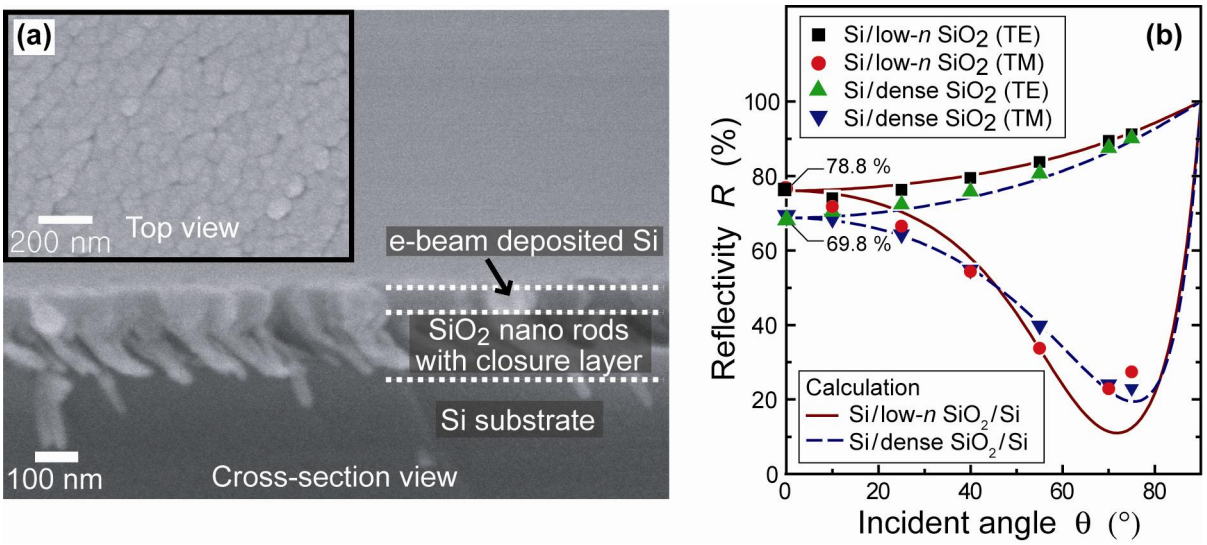

Fig. 10. (a) SEM of single-pair DBR incorporating SiO_2 nano-rod layer. (b) Measured and calculated TE and TM reflectivity of one-pair DBR using Si and either a dense SiO_2 or a low-*n* SiO_2 nanorod-array film.

The angular dependence of the reflectivity of the one-pair DBR structure is shown in Fig. 10(b). Inspection of the figure clearly reveals that the normal-incidence reflectivity is enhanced for the low-*n* DBR compared with the DBR using the dense SiO_2. The experimental normal-incidence reflectivity is 78.8% and 69.8% for the DBR using the low-*n* film and the dense SiO_2 film, respectively. The experimental results are in excellent agreement with the theoretical results using a refractive-index value of 1.08, 1.46 and 2.94 + 0.143 *i* for the low-*n* SiO_2, dense SiO_2 and Si, respectively.

3.3.3. Conductive ODR with nanorod ITO low-*n* layer

Although the semiconductor/SiO_2/Ag triple layer ODR shows higher reflectivity than the conventional DBRs and Ag reflectors, it needs an array of micro-contacts enabling electrical conductivity between the semiconductor and Ag through the *insulating* SiO_2 low-*n* layer, which leads to an increase in process complexity. In addition, the GaN-based ODR-LED needs absorptive *semi-transparent* current spreading layer, such as RuO_2, between SiO_2 and GaN,[3] which leads to a decrease in reflectivity of the ODR. Furthermore, the refractive index of SiO_2, n_{SiO2} = 1.46 at 468 nm, is not low enough for high refractive index contrast with high-index semiconductor materials, limiting further improvement of light-extraction efficiency in GaN-based LEDs. This motivates the development of ODR structure with new optical thin films with high *transparency*, high *conductivity*, and *low refractive index*. So, a conductive ODR consisting of GaN, Ag, and an intermediate indium-tin oxide (ITO) nanorod low-*n* layer is incorporated into a GaInN LED.

Optical thin films consisting of uniformly distributed ITO nanorods are grown by oblique-angle deposition of ITO by e-beam evaporation on Si substrate. The incident angle of vapor flux θ is about 80°. The evaporation source material is pure ITO granules. During the deposition, chamber pressure is 2×10^{-6} Torr, and deposition rate is well controlled at 0.5 nm/sec. Figure 11(a) shows the cross-sectional SEM graph for the ITO nanorod layer. The ITO nanorods are uniformly distributed with similar tilt angle of $\theta_t = 45°$. The gap between the SiO_2 nano rods is less than 50 nm, sufficiently small to limit optical scattering. AFM measurements were performed. Figure 12(b) shows AFM images of the ITO nanorods on Si substrate. The rms roughness of ITO nanorods is 6.1 nm.

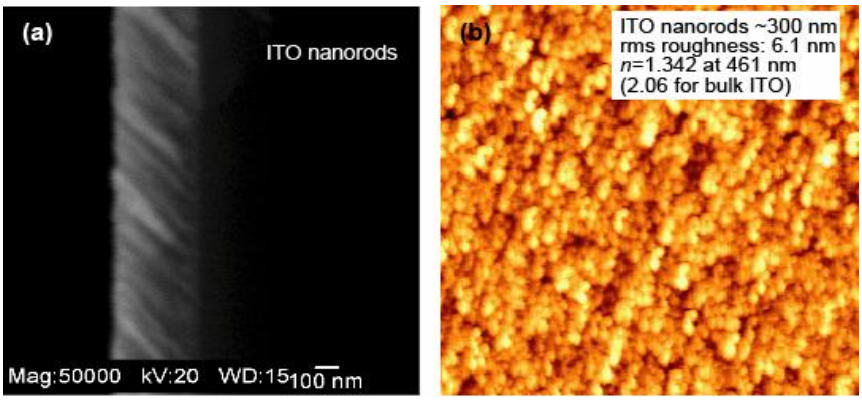

Fig. 11. (a) Cross-sectional view scanning electron microscopy graphs of ITO nanorod layer on Si substrate. (b) Atomic-force microscopy images of the surface of nanorod ITO layer.

The refractive index of this thin film is measured with ellipsometry. The sample is measured at multiple incident angles, 60°, 65°, and 70°. The ellipsometry model is Cauchy layer on Si substrate. The refractive index of the ITO nanorod layer is $n = 1.34$ at 461 nm. This value is much lower than the refractive index of dense ITO layer of $n = 2.06$ at 461 nm. The thickness of the ITO nanorod layer determined from the ellipsometry measurement is $h = 334$ nm, confirming the thickness obtained from SEM image (Fig. 11(a)). Generally, oblique-angle deposited thin films are anisotropic, the refractive index varying as a function of polarization as well as orientation with respect to the incident light wave. However, there is no obvious anisotropic property found in the ITO nanorod layer, possibly due to high porosity and the small thickness. The refractive index of a porous material is determined by the porosity and refractive index of the dense material. For two components with volume fractions V_{Air} and V_{ITO}, where $V_{\mathrm{Air}} + V_{\mathrm{ITO}} = 1$, and refractive indices n_{Air} and n_{ITO}, the Bruggemann effective-medium approximation gives[13]

$$V_{Air}\frac{n_{Air}^2 - n_{eff}^2}{n_{Air}^2 + 2n_{eff}^2} + (1 - V_{Air})\frac{n_{ITO}^2 - n_{eff}^2}{n_{ITO}^2 + 2n_{eff}^2} = 0 \qquad (7)$$

where n_{eff} is effective refractive index and V_{Air} is volume fraction of air (or porosity of film). The porosity V_{Air} of the low-n ITO layer is calculated to be 64.3 % using parameters, $n_{\mathrm{eff}} = 1.34$, $n_{\mathrm{ITO}} = 2.06$, and $n_{\mathrm{Air}} = 1$. A porous material has a refractive index related to the porosity and the refractive index of the original dense material. Such a low refractive index of 1.34 indicates that the ITO nanorod layer has the porosity about 68 %, while the SEM graphs appear to show porosity smaller than 68 %. We believe this is due to a possible porous structure in each nano rod, which cannot be seen clearly from the SEM images.

The low-n ITO is incorporated into a GaInN LED emitting at a peak wavelength of 474 nm. The GaInN LED structure was grown by metal-organic chemical vapor deposition on c-plane sapphire substrate and consists of a 3 μm-thick n-type GaN buffer layer, an n-type GaN lower cladding layer, a GaInN/GaN multiple quantum well active region, a p-type GaN upper cladding, and a highly doped GaN contact layer. A quarter-wave thick ITO nanorod layer was deposited by oblique-angle deposition of ITO using e-beam evaporation. The oblique incident angle is about 80°. In order to avoid the filling of e-beam evaporated ITO into the openings between the ITO nanorods, a very thin (20 nm) pore-closure layer is formed on the top surface of the ITO nanorod layer. After the pore-closure layer, 200 nm-thick Ag layer is deposited at normal incident angle of vapor flux by e-beam evaporation. LED mesa structures were obtained by standard photolithographic patterning followed by chemically-assisted ion-beam etching using Cl_2 and Ar to expose the n-type cladding layer. For comparison, LEDs with a Ag reflector were fabricated on the same wafer. Figures 12(a) and (b) show schematic cross-sectional views of the GaInN LED with Ag reflector and ODR with ITO nanorod low-refractive-index layer, respectively. The inset shows the SEM cross-sectional view of the ITO nanorods. The n-type contact for the samples was fabricated by electron-beam evaporation of Ti/Al/Ni/Au.

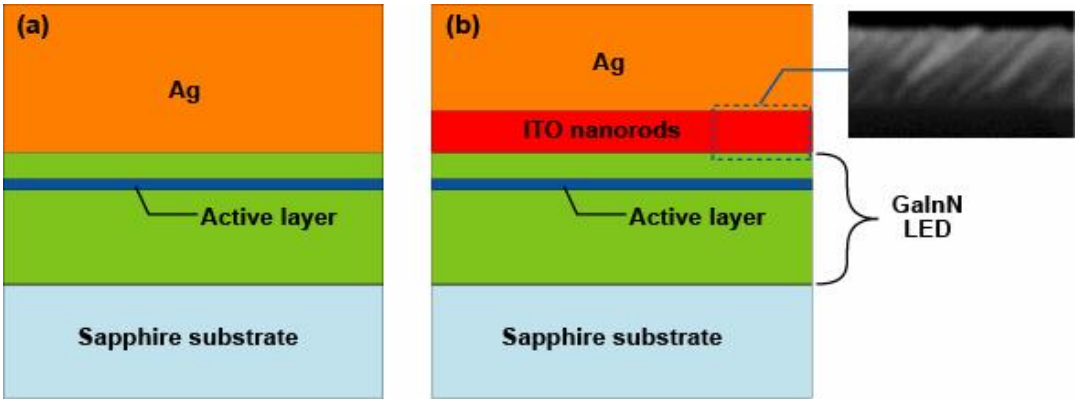

Fig. 12. Schematic cross-sectional view of GaInN LED with (a) Ag reflector and (b) GaN/ITO nanorods/Ag ODR. The inset shows the SEM cross-sectional view of the ITO nanorods.

Figure 13(a) shows the current-voltage characteristics of the LED with GaN/ITO nanorods/Ag ODR and the LEDs with Ag contacts. The forward voltage at 20 mA for the LED with GaN/ITO nanorods/Ag ODR is 3.5 V. On the other hand, the forward voltage of the LED with Ag contact is as high as 7.5 V. This is due to a low work function of Ag, resulting in a high potential barrier between Ag and p-type GaN. The electroluminescence intensity from the backsides of the LEDs was measured directly on a large-size (10×10 mm^2) Si PIN photodetector. The light-output–versus-current characteristic of the LEDs is shown in Fig. 13(b). The light-output power from the LEDs with GaN/ITO nanorods/Ag ODR is significantly higher than those from the LEDs with Ag contact. At an injection current of 20 mA, the enhancement in light-output of the LEDs with GaN/low-*n* ITO/Ag ODR is 31.6 % compared to the LEDs with Ag reflector. The increased light output of the LED with GaN/ITO nanorods/Ag ODR can be attributed to higher reflectivity, and hence better light-extraction efficiency due to the use of the ITO nanorods as low-*n* layer.

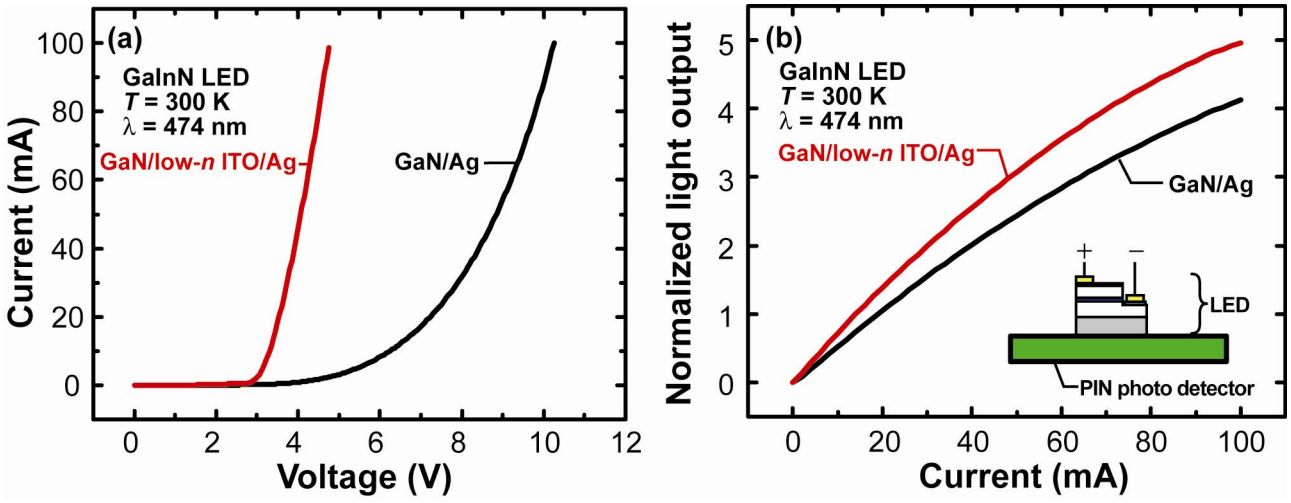

Fig. 13. (a) Current-voltage characteristics and (b) light output vs drive current characteristic of GaInN LED with GaN/ITO nanorods/Ag ODR and LED with Ag contacts. The light output from the backsides of the LEDs was measured directly on a large-size blue-enhanced Si PIN photodetector.

4. Summary

In summary, we presented enhanced light output in GaN blue LEDs by employing ODRs. ODRs significantly increase the light extraction from the AlGaInP-based and GaInN-based LEDs as compared to reference LEDs employing DBR or metal reflector. Further improvements of reflectivity were achieved by using novel low-*n* materials such as nanoporous SiO_2 fabricated by a sol-gel process, nanorod SiO_2 and indium-tin oxide (ITO) layers fabricated by oblique-angle deposition technique. SiO_2 nanorod-array dielectric films with unprecedented low refractive indices of 1.08 are

demonstrated and shown to have viable optical properties including enhanced reflectivity of a single-pair DBR. In addition, an array of ITO nanorods is deposited by oblique-angle deposition using e-beam evaporation. The refractive index of the ITO nanorod layer is 1.34 at 461 nm, significantly lower that that of dense ITO, n = 2.06 at 461 nm. Incorporation of low-n ITO layer into GaInN LEDs results in further improvement of reflectivity, and hence light-output of the ODR-LEDs due to a high refractive index contrast. The light output of the GaN LED with GaN/ITO nanorods/Ag ODR is 31.6% higher than that of the LEDs with Ag reflector. This is attributed to enhanced reflectivity of the ODR by using ITO nanorod low-refractive-index layer with high transparency, high conductivity, and low refractive index.

Acknowledgement

We gratefully acknowledge support from National Science Foundation (NSF), the Defense Advanced Research Projects Agency (DARPA), the Army Research Office (ARO), Crystal IS Corporation, and Samsung Advanced Institute of Technology (SAIT).

References

1. T. Gessmann, E. F. Schubert, J. W. Graff, K. Streubel, and C. Karnutsch, "Omnidirectional Reflective Contacts for Light-Emitting Diode," *IEEE Elec. Dev. Lett.*, **24**, 683 (2003).
2. T. Gessmann and E. F. Schubert, "High-efficiency AlGaInP light-emitting diodes for solid-state lighting applications," *J. Appl. Phys.* **95**, 2203 (2004).
3. J. K. Kim, T. Gessmann, H. Luo, and E. F. Schubert, "GaInN light-emitting diodes with RuO_2/SiO_2/Ag omni-directional reflector," *Appl. Phys. Lett.* **84**, 4508 (2004).
4. M. Born and E. Wolf, *Principle of Optics 6th edition*, p. 62, Pergamon Press, (1987).
5. M. R. Krames *et al*., "High-power truncated-inverted-pyramid $(Al_xGa_{1-x})_{0.5}In_{0.5}P$/GaP light-emitting diodes exhibiting > 50 % external quantum efficiency," *Appl. Phys. Lett.* **75,** 2365 (1999).
6. N. F. Gardner *et al*., "1.4× improvement in transparent substrate $(Al_xGa_{1-x})_{0.5}In_{0.5}P$/GaP light-emitting diodes with thin (≤200 nm) active regions," *Appl. Phys. Lett.* **74,** 2230 (1999).
7. S. V. Nitta, V. Pisupatti, A. Jain, P. C. Wayner, Jr., W. N. Gill, and J. L. Plawsky, "Surface modified spin-on xerogel films as interlayer dielectrics," *J. Vac. Sci. Technol. B* **17**, 205 (1999).
8. J.-Q. Xi, M. Ojah, W. Cho, T. Gessmann, E. F. Schubert, J. L. Plawsky, and W. N. Gill, "Omnidirectional reflector using nanoporous SiO_2 as a low-refractive index material," *Opt. Lett.* **30**, 1518 (2005).
9. M. Schmidt *et al.*, "Ultra-low refractive index substrates–a base for photonic crystal slab waveguides," *Appl. Phys. Lett.* **85**, 16 (2004).
10. J.-Q. Xi, Jong Kyu Kim, and E. Fred Schubert, "Silica nanorod-array films with very low refractive indices," *Nano Letters* **5**, 1385 (2005).
11. K. Robbie, M. J. Brett, "Sculptured thin films and glancing angle deposition: Growth mechanics and applications", *J. Vac. Sci. Technol. A* **15**, 1460 (1997).
12. D. Vick *et al*., "Self-shadowing and surface diffusion Effects in obliquely-deposited thin films", *Thin Solid Films* **339**, 88 (1999).
13. K. H. H. Peter, T. D. Stephen, H. F. Richard, T. Nir, "All-polymer optoelectronic devices," Science **285**, 233 (1999).